

Revealing the Origin of Time-reversal Symmetry Breaking in Fe-chalcogenide Superconductor $\text{FeTe}_{1-x}\text{Se}_x$

Camron Farhang¹, Nader Zaki², Jingyuan Wang¹, Genda Gu², Peter D. Johnson² and Jing Xia¹

¹*Department of Physics and Astronomy, University of California, Irvine, California 92697, USA*

²*Condensed Matter Physics and Materials Science Division (CMPMSD), Brookhaven National Laboratory, Upton, NY 11973*

Recently evidence has emerged in the topological superconductor Fe-chalcogenide $\text{FeTe}_{1-x}\text{Se}_x$ for time-reversal symmetry breaking (TRSB), the nature of which has strong implications on the Majorana zero modes (MZM) discovered in this system. It remains unclear however whether the TRSB resides in the topological surface state (TSS) or in the bulk, and whether it is due to an unconventional TRSB superconducting order parameter or an intertwined order. Here by performing in superconducting $\text{FeTe}_{1-x}\text{Se}_x$ crystals both surface-magneto-optic-Kerr effect (SMOKE) measurements using a Sagnac interferometer and bulk magnetic susceptibility measurements, we pinpoint the TRSB to the TSS, where we also detect a Dirac gap. Further, we observe surface TRSB in non-superconducting $\text{FeTe}_{1-x}\text{Se}_x$ of nominally identical composition, indicating that TRSB arises from an intertwined surface ferromagnetic (FM) order. The observed surface FM bears striking similarities to the two-dimensional (2D) FM found in 2D van der Waals crystals, and is highly sensitive to the exact chemical composition, thereby providing a means for optimizing the conditions for Majorana particles that are useful for robust quantum computing.

The quest for a robust quantum computer that is immune to external perturbations has stimulated intense searches for topologically protected quantum phases of matter where quasiparticles obey non-Abelian exchange rules [1]. One such example, the Majorana zero modes (MZM), have been reported in Fe-chalcogenide superconductors $\text{FeTe}_{1-x}\text{Se}_x$ as bound states in magnetic vortex cores [2–5] and as propagating 1D modes [6] by scanning tunnelling microscopy (STM) that performs spectroscopic imaging of the surface state. However, the imperfect conductance quantization [5] and the unexpected field dependence of MZM's occurrence [4] highlight the need for a deeper understanding of $\text{FeTe}_{1-x}\text{Se}_x$ towards the optimization of material conditions for MZM. The hallmark of topological superconductivity [7], the topological surface state (TSS) has been reported [8,9] in $\text{FeTe}_{1-x}\text{Se}_x$ by angle-resolved photo emission spectroscopy (ARPES) that probes the energy dispersions of surface electrons. Photoemission spectra reveal [8,9] a topologically protected TSS characterized by a linear dispersion centered at the Dirac point at chemical potential μ below E_F , and below the superconducting critical temperature T_c , a superconducting gap at the Fermi energy E_F . It is this superconducting TSS, when subjected to a magnetic field, that hosts the reported MZM that is potentially useful for topologically protected quantum computing. Without the magnetic field, the TSS is expected to obey time-reversal symmetry (TRS) and remain massless.

Therefore, it came as a surprise when in a low temperature ARPES study at zero magnetic field [10] the above linear dispersion was interrupted by the opening of a Dirac gap as temperature is lowered across T_c in $\text{FeTe}_{1-x}\text{Se}_x$. The associated mass acquisition points to symmetry breaking. To explain this observation, a phenomenological Weiss field h was introduced to the surface Hamiltonian, which fits well to the observed photoemission spectra [10]. A Weiss field in

the absence of an external magnetic field represents spontaneous time-reversal symmetry breaking (TRSB), which could arise from ferromagnetism (FM) or an intrinsic TRSB superconducting (SC) state [11]. So far, the results of magnetic characterizations of $\text{FeTe}_{1-x}\text{Se}_x$ remain mixed. While nitrogen vacancy center (NV) magnetometry has detected static magnetic fields that are best described by a combination of SC supercurrents and FM in micron-sized exfoliated flakes [12], high resolution magnetic neutron scattering measurements of bulk crystals have revealed instead antiferromagnetic (AFM) orders of either double or single stripe spin arrangements [13]. Since ARPES is surface sensitive while NV magnetometry and neutron scattering probe predominantly the bulk, a critical step to solve this mystery is to separately identify the TRSB properties of the bulk and surface in $\text{FeTe}_{1-x}\text{Se}_x$. Another central issue is to resolve the relation between the possible TRSB and the SC order: is TRSB from a FM phase that competes with the SC; or does the SC state in $\text{FeTe}_{1-x}\text{Se}_x$ have an intrinsically TRSB order parameter analogous to the superfluidity [14] in He^3 ? If it is the first case, one might be able to separately control the FM and SC orders in the surface and engineer the optimal conditions for MZM in vortex cores. And the second scenario points to a new unconventional SC state. Based on ARPES spectra taken at discrete temperatures [10], the Dirac gap in TSS opens at a temperature close to T_c . Therefore the second scenario was favored in prior theoretical treatments [11], but needs to be tested by stringent experiments.

Surface-magneto-optic-Kerr effect (SMOKE) [15,16] measurements performed by a zero-area loop fiber optic Sagnac interferometer [17] are ideally suited for addressing these questions. In a conventional SMOKE setup, a linearly polarized light beam interacts with the surface magnetic moment M through spin-orbit coupling and will experience a rotation θ_K of the polarization plane [18]. The Kerr rotation

θ_K is proportional to M , and thus provides a direct measurement of surface magnetization within the optical penetration depth δ , typically a few nanometers for conductors [15,16]. For even higher resolution, we have introduced a zero-area loop [17] fiber optic Sagnac interferometer [19] that measures directly the non-reciprocal phase difference between counter-propagating circularly polarized light beams. It fundamentally rejects polarization rotations due to non-TRSB effects such as linear and circular dichroism [20].

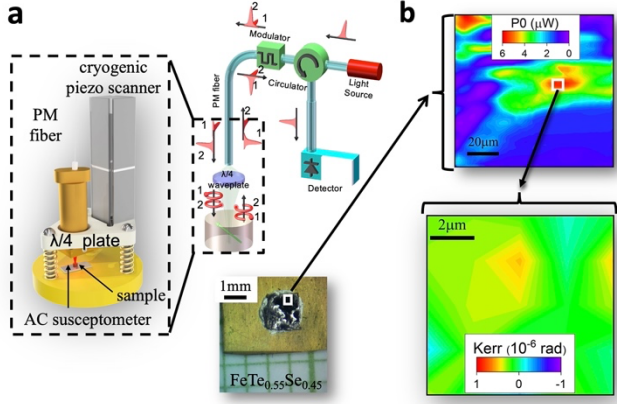


Fig. 1. (a) Sagnac setup for polar Kerr measurements (b) Scanning images of reflected optical power P_0 and Kerr signal (θ_K) of a $\text{FeTe}_{0.55}\text{Se}_{0.45}$ sample (type B) at 1.8 K and zero magnetic field.

As illustrated in Fig. 1a, for this study we utilize a scanning Sagnac microscope with $2 \mu\text{m}$ lateral spatial resolution [21,22], inside a cryostat with 1.8 K base temperature and 9 T magnetic field capability. The interferometer itself is maintained at room temperature. And a polarization maintaining fiber delivers light beams of orthogonal linear polarizations into the high vacuum sample space inside the cryostat. A cryogenic quarter wave ($\lambda/4$) plate converts the polarization of these light beams to circular polarization of opposite chirality that will interact with the sample surface and detect TRSB in the form of the non-reciprocal phase difference $\phi_{nr} = 2\theta_K$ when they finish the Sagnac loop and interfere at the detector. The Kerr resolution is at the ten nanoradian ($n\text{rad}$) level [23,24] that is about a thousand times better than conventional SMOKE [15,16]. The ARPES studies were carried out using the frequency quadrupled output of a 3-ps pulse width, 76-MHz repetition rate Coherent Mira 900P Ti:sapphire laser. The photoemission spectra were obtained using a Scienta SES 2002 electron spectrometer with an effective energy resolution of 2.5 meV. Bulk magnetic characterizations are performed using an AC susceptometer. Instrumentation details are presented in the Supplementary Information (FIG. S1-S3).

Single crystals of $\text{FeTe}_{1-x}\text{Se}_x$ with nominal x values of 0.3 and 0.45 were grown by a unidirectional solidification

method (Supplementary Information FIG. S5). Flat ab plane surface regions of tens of microns in size can be found (Fig. 1a inset) for measurements. We locate such flat regions with uniform reflected optical power (P_0) before performing spatial Kerr (θ_K) scans at a fixed temperature or temperature scans at a fixed location. Fig. 1b demonstrates an example of this experimental procedure for a $\text{FeTe}_{0.55}\text{Se}_{0.45}$ sample. In the flat region inside the white square with a uniform $P_0 = 6 \mu\text{W}$, the Kerr scan shows a signal of up to $\theta_K = 500 n\text{rad}$ at the base temperature of 1.8 K and zero magnetic field, indicating spontaneous TRSB. As is typical of spontaneous symmetry breaking, the sign and size of θ_K at zero magnetic field normally varies as a function of location and temperature, which agrees with the Kerr scan in Fig. 1b.

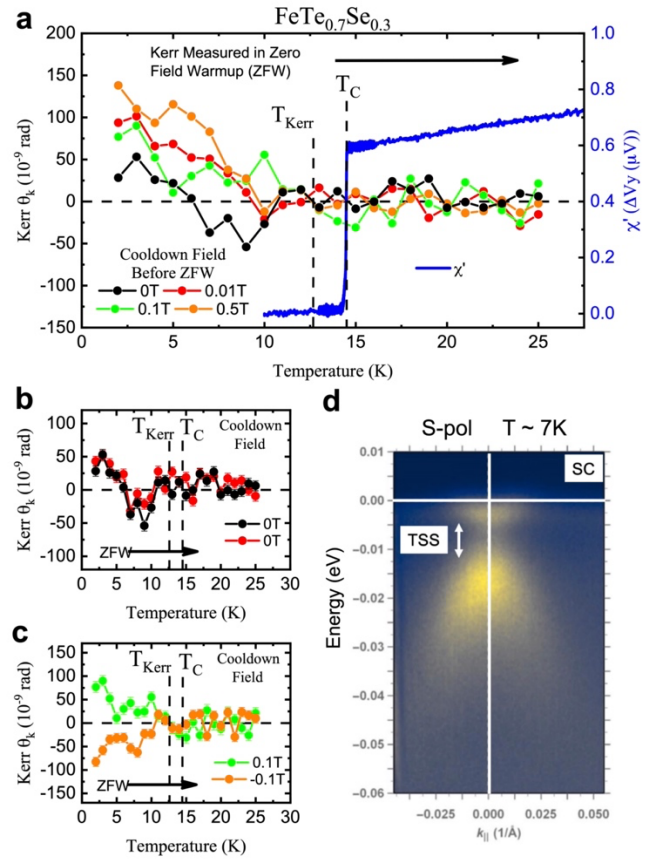


Fig. 2. Superconducting $\text{FeTe}_{0.7}\text{Se}_{0.3}$ (a) Kerr θ_K (left axis) up to $150 n\text{rad}$ during zero field warmups (ZFW) indicate onset of spontaneous TRSB at T_{Kerr} ; bulk magnetic susceptibility χ' (right axis) indicates onset of SC at T_C without any sign of bulk FM. (b) θ_K during ZFW after zero field cooldown. (c) θ_K during ZFW after $\pm 0.1\text{T}$ trainings during cooldown. (d) ARPES spectral intensity measured in the vicinity of the Γ -point ($k_{||} = 0$), using s-polarized light and with the sample in the superconducting state at 7 K.

To pinpoint the location of the observed TRSB, we first focus on a $\text{FeTe}_{0.7}\text{Se}_{0.3}$ sample that was studied by ARPES

in the prior publication [10] where a Dirac gap opens below the superconducting critical temperature $T_c = 14 K$. This Dirac gap in the TSS can be seen in the 7 K ARPES spectral intensity map with s-polarized light in Fig. 2d. Bulk superconductivity is verified in AC susceptibility measurements (right axis, blue line) shown in Fig. 2a, where χ' displays a pronounced sharp diamagnetic Meissner drop when the sample is cooled below $T_c = 14 K$. There is no sign in $\chi'(T)$ of any bulk FM transition, which agrees with magnetic neutron scattering [13]. In contrast, the surface Kerr signal measured during zero magnetic field warmups (ZFW) after zero magnetic field cooling (ZFC), as shown in Fig. 2b, display clear onsets of θ_K at $T_{Kerr} = 12.5 K$. This serves as direct evidence of TRSB on the surface, either due to the formation of surface FM, or an unconventional TRSB SC state. As explained earlier, the sign and size of spontaneous θ_K are normally not fixed during ZFW after ZFC. Indeed in Fig. 2b polar Kerr signals θ_K of up to $\pm 50 nrad$ have their sign fluctuating between positive and negative. In exfoliated flakes with a large surface-to-volume ratio, the TRSB surface might generate a magnetic field that is comparable in size to that from bulk SC, and account for the detected static field by nitrogen vacancy center (NV) magnetometry [12]. The AC susceptibility and surface Kerr measurements are consistent with ARPES spectra taken at 7 K (Fig. 2d) that shows the coexistence of the SC gap at $E_F = 0 meV$ and the Dirac gap at the Dirac point of $-0.008 eV$. We note that T_{Kerr} and T_c are close to each other within 1.5 K, and are difficult to distinguish in prior experiments [10,13]. We shall describe a decisive experiment later in this paper to tell them apart.

The sign of θ_K can be trained by cooling down in a symmetry-breaking magnetic field $B_{Cooling}$. This is demonstrated in Fig. 2c where $B_{Cooling} = \pm 0.1 T$ during cooldowns result in $\pm 100 nrad$ of spontaneous Kerr signal in subsequent ZFWs. In the case of FM, this is the well-known alignment of FM domains by an external magnetic field [25]. This training effect has also been demonstrated in TRSB superconductors [23,24,26,27], but with an important caveat. In a type II superconductor such as $FeTe_{1-x}Se_x$, magnetic vortices form when $B_{Cooling}$ is larger than the lower critical field H_{C1} and penetrates the superconductor. After removal of $B_{Cooling}$, a small fraction of vortices can still be trapped at pinning sites, resulting in Kerr signals during ZFW. In fact, we speculate that motions of trapped vortices under thermal gradients may account for the reported spontaneous Nernst signal [28] in $FeTe_{1-x}Se_x$. Since H_{C1} of 4 mT [29] is smaller than the coercive field, in this sample trainings involve trapped vortices. To tell whether their contributions dominate θ_K , Kerr signals were measured during ZFW after training fields of 0.01, 0.1 and 0.5 T as shown in Fig. 2a. We expect the number of trapped vortices hence their contributions to θ_K to roughly scale with training fields. However, remanent θ_K at $T = 1.8 K$ only differ between 80 to 140 nrad despite the 50 times difference in

training fields, indicating that the trained θ_K in this sample are not dominated by trapped vortices.

Now we have experimentally established that TRSB occurs only on the surface, we turn to experiments on samples with the nominal chemical composition of $FeTe_{0.55}Se_{0.45}$ to identify the origin of this surface TRSB. Recently neutron scattering, ARPES, and resistivity measurements have been carried out to establish that $FeTe_{0.55}Se_{0.45}$ is located very close to phase boundaries in a complex phase diagram [13]. By a few percent change of the Fe concentration, at $T = 0$ a nominal $FeTe_{0.55}Se_{0.45}$ can be a non-superconductor (Type A), a SC with TSS (Type B), or a trivial SC without TSS [13]. In a Type A sample, neutron scattering has revealed a double stripe spin arrangement for the bulk AFM order, and the APRES spectra are featureless; while in a Type B sample, a single stripe spin arrangement is found, and the APRES spectra show both SC and TSS states.

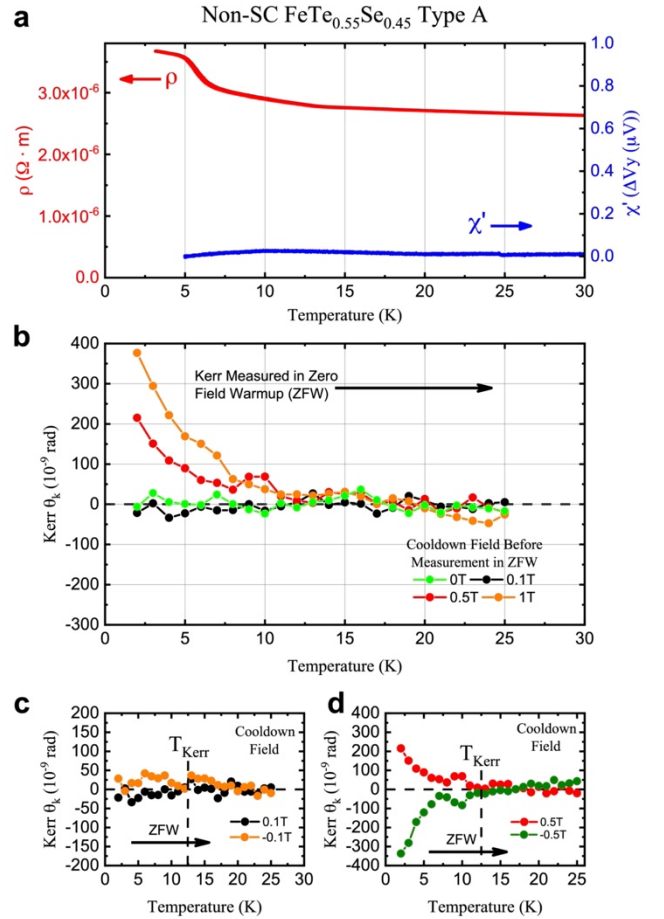


Fig. 3. Non-superconducting $FeTe_{0.55}Se_{0.45}$ (Type A) (a) Resistivity ρ and bulk magnetic susceptibility χ' show no sign of SC or bulk FM transitions; (b) θ_K up to 400 nrad during ZFW indicates onset of surface FM at T_{Kerr} ; (c) θ_K during ZFW after $\pm 0.1 T$ trainings. (d) θ_K during ZFW after $\pm 0.5 T$ trainings.

We have performed measurements on both types of $FeTe_{0.55}Se_{0.45}$ samples. The experimental results on a Non-

SC (Type A) $\text{FeTe}_{0.55}\text{Se}_{0.45}$ sample are summarized in Fig. 3, where the ARPES spectra are featureless indicating the absence of TSS. And those on a SC+TSS (Type B) $\text{FeTe}_{0.55}\text{Se}_{0.45}$ sample are summarized in Fig. 4, with a Dirac gap in TSS and a SC gap at E_F in the ARPES spectra (Fig. 4d) at $T \sim 5 \text{ K}$.

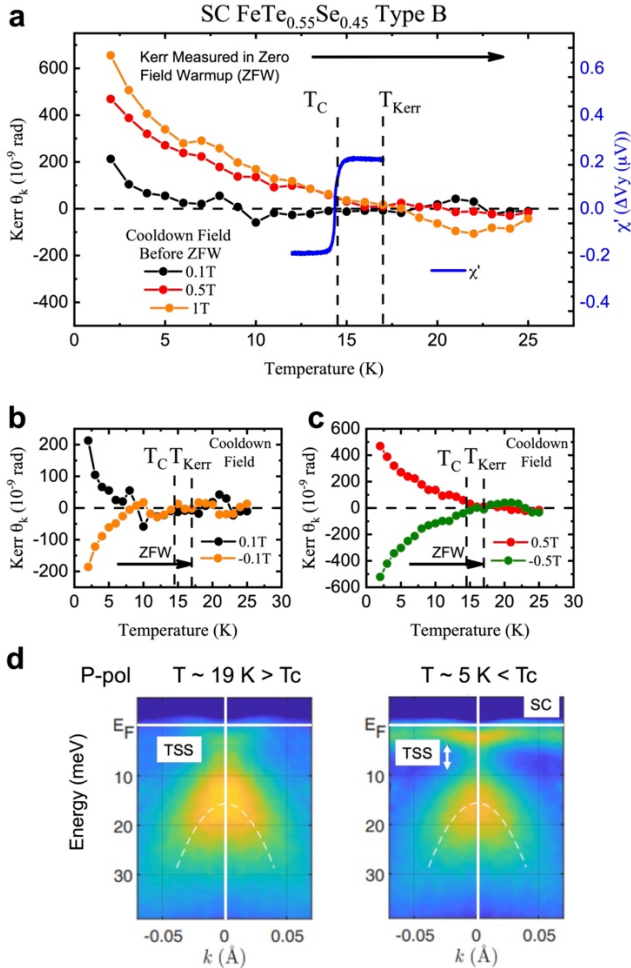


Fig. 4. Superconducting $\text{FeTe}_{0.55}\text{Se}_{0.45}$ (Type B) (a) θ_K (left axis) up to 600 nrad during ZFW indicates onset of TRSB at T_{Kerr} ; bulk magnetic susceptibility χ' (right axis) indicates onset of SC at T_C without any sign of bulk FM. (b) θ_K during ZFW after $\pm 0.1 \text{ T}$ trainings. (c) θ_K during ZFW after $\pm 0.5 \text{ T}$ trainings. (d) ARPES spectral intensity measured in the vicinity of the Γ -point ($k_{\parallel} = 0$), using p-polarized light, showing TSS at all temperatures, and the opening of a SC gap below T_C .

As shown in Fig. 3a, in the non-SC type A sample, the resistivity ρ shows no sign of SC either in the bulk or on the surface. Magnetic susceptibility χ' confirms that there is no bulk SC, and it shows no sign of any bulk FM transition. Comparing the size of χ' in this non-SC sample to the drop of χ' across T_C in the SC type B sample (Fig. 4a), we can estimate an upper bound of 1% for superconducting volume

fraction, indicating that this type A sample is indeed deep in the non-SC region of the phase diagram [13]. Therefore, the onsets of the surface Kerr signal up to $\theta_K = 400 \text{ nrad}$ (Fig. 3b) during ZFW undoubtedly indicate that the observed surface TRSB is not due to a TRSB order parameter of the SC state. Instead, it originates from surface FM. In a non-SC sample (Fig. 3), $T_{Kerr} > 0$ and $T_C = 0$; while in superconducting samples (Fig. 2 and Fig. 4), T_{Kerr} and T_C are not necessarily identical, but they are close to each other. The observed closeness between T_{Kerr} and T_C , being a mere coincidence or not, puts the competing FM and SC orders very close in energy, and may be partially responsible for the complex phase diagram [13].

Note that there is no contribution to θ_K from trapped vortices for the entire temperature range in the Type A sample, and for $T_C < T < T_{Kerr}$ in the Type B sample. With the absence of any bulk FM signal, these two samples further confirm surface localization of TRSB.

The temperature dependences of the spontaneous Kerr signal θ_K (Fig. 2a, Fig. 3a, and Fig. 4a) in $\text{FeTe}_{1-x}\text{Se}_x$ bare striking similarities to the two-dimensional (2D) ferromagnetism in 2D van der Waals (vdW) crystals of $\text{Cr}_2\text{Ge}_2\text{Te}_6$, especially the bilayer case [21] (Supplementary Information FIG. S4). Namely, $\theta_K(T)$ doesn't saturate quickly with a reduced temperature following the well-known $\tanh\left(\frac{\mu B_E}{k_B T}\right)$ function of the 3D Heisenberg model [25], where B_E is the molecular field. Instead, like in the exfoliated bilayers of $\text{Cr}_2\text{Ge}_2\text{Te}_6$, $\theta_K(T)$ appears to keep growing at the lowest temperatures [21], which is a direct consequence of the fact that 2D magnetism is stabilized by magnetic anisotropy instead of magnetic exchange coupling [21]. The surface FM in $\text{FeTe}_{1-x}\text{Se}_x$ is sensitive to the chemical composition, indeed, the amplitude of observed spontaneous θ_K in $\text{FeTe}_{0.55}\text{Se}_{0.45}$ of both type A and B are four times larger than in $\text{FeTe}_{0.7}\text{Se}_{0.3}$. In addition, while a training field of a mere 0.01 T is enough to achieve a saturating θ_K in $\text{FeTe}_{0.7}\text{Se}_{0.3}$, 0.5 T is needed in $\text{FeTe}_{0.55}\text{Se}_{0.45}$ samples. The fifty times difference in coercivity suggests a large difference in the magnetic anisotropy between $\text{FeTe}_{0.55}\text{Se}_{0.45}$ and $\text{FeTe}_{0.7}\text{Se}_{0.3}$. In contrast, the SC and FM onset temperatures T_C and T_{Kerr} only shift by a few Kelvins between $\text{FeTe}_{0.7}\text{Se}_{0.3}$ and SC $\text{FeTe}_{0.55}\text{Se}_{0.45}$. While it is premature to speculate on the origin of the surface FM, we note that magnetism could occur at surfaces and interfaces where inversion symmetry is broken [30].

In summary, we have unambiguously identified TRSB in $\text{FeTe}_{1-x}\text{Se}_x$ and pinpoint its origin to be surface ferromagnetism. The detected polar Kerr signals at zero magnetic fields indicate a perpendicular component of the surface magnetization, which is necessary to form the observed Dirac gap. The surface FM is highly sensitive to the exact chemical composition, which would allow exploring the optimal conditions for stabilizing MZM in magnetic vortex cores [2–5] and 1D modes [6] useful for quantum computing [1].

We acknowledge discussions with C. Wu and I. Zaliznyak. This project was supported mainly by NSF award DMR-1807817, and in part by the Gordon and Betty Moore Foundation through Grant GBMF10276. The work at BNL

email: xia.jing@uci.edu

- [1] C. Nayak, S. H. Simon, A. Stern, M. Freedman, and S. Das Sarma, *Non-Abelian Anyons and Topological Quantum Computation*, Reviews of Modern Physics **80**, 1083 (2008).
- [2] D. Wang et al., *Evidence for Majorana Bound States in an Iron-Based Superconductor*, Science **362**, 333 (2018).
- [3] L. Kong et al., *Half-Integer Level Shift of Vortex Bound States in an Iron-Based Superconductor*, Nat. Phys. **15**, 1181 (2019).
- [4] T. Machida, Y. Sun, S. Pyon, S. Takeda, Y. Kohsaka, T. Hanaguri, T. Sasagawa, and T. Tamegai, *Zero-Energy Vortex Bound State in the Superconducting Topological Surface State of Fe(Se,Te)*, Nat. Mater. **18**, 811 (2019).
- [5] S. Zhu et al., *Nearly Quantized Conductance Plateau of Vortex Zero Mode in an Iron-Based Superconductor*, Science **367**, 189 (2020).
- [6] Z. Wang, J. O. Rodriguez, L. Jiao, S. Howard, M. Graham, G. D. Gu, T. L. Hughes, D. K. Morr, and V. Madhavan, *Evidence for Dispersing 1D Majorana Channels in an Iron-Based Superconductor*, Science **367**, 104 (2020).
- [7] X.-L. Qi and S. Zhang, *Topological Insulators and Superconductors*, Reviews of Modern Physics **83**, 1057 (2011).
- [8] P. Zhang et al., *Observation of Topological Superconductivity on the Surface of an Iron-Based Superconductor*, Science **360**, 182 (2018).
- [9] J. D. Rameau, N. Zaki, G. D. Gu, P. D. Johnson, and M. Weinert, *Interplay of Paramagnetism and Topology in the Fe-Chalcogenide High- T_c Superconductors*, Phys. Rev. B **99**, 205117 (2019).
- [10] N. Zaki, G. Gu, A. Tsvelik, C. Wu, and P. D. Johnson, *Time-Reversal Symmetry Breaking in the Fe-Chalcogenide Superconductors*, Proc. Natl. Acad. Sci. U.S.A. **118**, e2007241118 (2021).
- [11] L.-H. Hu, P. D. Johnson, and C. Wu, *Pairing Symmetry and Topological Surface State in Iron-Chalcogenide Superconductors*, Phys. Rev. Research **2**, 022021 (2020).
- [12] N. J. McLaughlin et al., *Strong Correlation Between Superconductivity and Ferromagnetism in an Fe-Chalcogenide Superconductor*, Nano Lett. **21**, 7277 (2021).
- [13] Y. Li et al., *Electronic Properties of the Bulk and Surface States of Fe $_{1+y}$ Te $_{1-x}$ Sex*, Nat. Mater. **20**, 9 (2021).
- was supported by the US Department of Energy, office of Basic Energy Sciences, contract no. DOE-sc0012704.
- [14] A. J. Leggett, *A Theoretical Description of the New Phases of Liquid He $_3$* , Reviews of Modern Physics **47**, 331 (1975).
- [15] Z. Qiu, *Surface Magneto-Optic Kerr Effect (SMOKE)*, Journal of Magnetism and Magnetic Materials **200**, 664 (1999).
- [16] S. D. Bader, *Smoke*, Journal of Magnetism and Magnetic Materials **100**, 440 (1991).
- [17] J. Xia, P. T. Beyersdorf, M. M. Fejer, and A. Kapitulnik, *Modified Sagnac Interferometer for High-Sensitivity Magneto-Optic Measurements at Cryogenic Temperatures*, Applied Physics Letters **89**, (2006).
- [18] P. Weinberger, *John Kerr and His Effects Found in 1877 and 1878*, Philosophical Magazine Letters **88**, 897 (2008).
- [19] G. Sagnac, *On the Proof of the Reality of the Luminiferous...*, Comptes Rendus (1913).
- [20] A. Kapitulnik, J. Xia, E. Schemm, and A. Palevski, *Polar Kerr Effect as Probe for Time-Reversal Symmetry Breaking in Unconventional Superconductors*, New Journal of Physics **11**, (2009).
- [21] C. Gong et al., *Discovery of Intrinsic Ferromagnetism in Two-Dimensional van Der Waals Crystals*, Nature **546**, 265 (2017).
- [22] S. Thomas et al., *Localized Control of Curie Temperature in Perovskite Oxide Film by Capping-Layer-Induced Octahedral Distortion*, Phys. Rev. Lett. **119**, 177203 (2017).
- [23] J. Xia, Y. Maeno, P. T. Beyersdorf, M. M. Fejer, and A. Kapitulnik, *High Resolution Polar Kerr Effect Measurements of Sr 2 RuO $_4$: Evidence for Broken Time-Reversal Symmetry in the Superconducting State*, Physical Review Letters **97**, (2006).
- [24] X. Gong, M. Kargarian, A. Stern, D. Yue, H. Zhou, X. Jin, V. M. Galitski, V. M. Yakovenko, and J. Xia, *Time-Reversal Symmetry-Breaking Superconductivity in Epitaxial Bismuth/Nickel Bilayers*, Sci. Adv. **3**, e1602579 (2017).
- [25] C. Kittel, *Introduction to Solid State Physics* (Wiley, 2004).
- [26] E. R. Schemm, W. J. Gannon, C. M. Wishne, W. P. Halperin, and A. Kapitulnik, *Observation of Broken Time-Reversal Symmetry in the Heavy-Fermion Superconductor UPt $_3$* , Science **345**, 190 (2014).
- [27] I. M. Hayes et al., *Multicomponent Superconducting Order Parameter in UTe $_2$* , Science **373**, 797 (2021).
- [28] L. Chen, Z. Xiang, C. Tinsman, B. Lei, X. Chen, G. D. Gu, and L. Li, *Spontaneous Nernst Effect in the Iron-Based Superconductor Fe $_{1+y}$ Te $_{1-x}$ Sex*, Phys. Rev. B **102**, 054503 (2020).

- [29] M. Bendele et al., *Anisotropic Superconducting Properties of Single-Crystalline FeTe_{0.5}Se_{0.5}*, Phys. Rev. B **81**, 224520 (2010).
- [30] F. Hellman et al., *Interface-Induced Phenomena in Magnetism*, Rev. Mod. Phys. **89**, 025006 (2017).
- [31] See Supplemental Material [url] for additional experimental information, which includes

Refs. [32-36].

- [32] D. Low, G. M. Ferguson, A. Jarjour, B. T. Schaefer, M. D. Bachmann, P. J. W. Moll, and K. C. Nowack, *Scanning SQUID Microscopy in a Cryogen-Free Dilution Refrigerator*, Review of Scientific Instruments **92**, 083704 (2021).
- [33] M. Nikolo, *Superconductivity: A Guide to Alternating Current Susceptibility Measurements and Alternating Current Susceptometer Design*, American Journal of Physics **63**, 57 (1995).
- [34] L. J. van der Pauw, *A Method of Measuring Specific Resistivity and Hall Effect of Discs of Arbitrary Shape*, in *Semiconductor Devices: Pioneering Papers* (WORLD SCIENTIFIC, 1991), pp. 174–182.
- [35] J. Luo, T. P. Orlando, J. M. Graybeal, X. D. Wu, and R. Muenchausen, *Scaling of the Longitudinal and Hall Resistivities from Vortex Motion in YBa₂Cu₃O₇*, Phys. Rev. Lett. **68**, 690 (1992).
- [36] A. T. Dorsey, *Vortex Motion and the Hall Effect in Type-II Superconductors: A Time-Dependent Ginzburg-Landau Theory Approach*, Phys. Rev. B **46**, 8376 (1992).